Ceramics-Silikáty 67 (3), 379-386 (2023)
www.ceramics-silikaty.cz doi: 10.13168/cs.2023.0038

EXPERIMENTAL AND DFT STUDY ON THE EFFECTS OF Mn DOPING ON THE STRUCTURAL AND OPTICAL PROPERTIES OF CUO NANOPARTICLES

#H. A. KASSIM, KHALID ELFAKI IBRAHIM

*Department of Physics, College of Science, P.O. BOX 2455, King Saud University, Riyadh 11451, Saudi Arabia

#E-mail: hkassim@ksu.edu.sa

Submitted July 29, 2023; acceptedAugust 30, 2023

Keywords: Nanoparticles, Monoclinic, Bandgap, Density of state, Band structure

Nanoparticles doped with transition metal elements have attracted considerable interest due to their unique physical and chemical properties, which can be finely tuned for diverse applications. This study looks at the structural and optical properties of manganese (Mn)-doped copper oxide (CuO) nanoparticles. X-ray diffraction (XRD) and the Rietveld refinement analysis revealed a well-monoclinic structure without a second phase, indicating successful doping without significant changes in the CuO crystal lattice. The scanning electron microscope (SEM) images show that the pure and Mn-doped CuO nanoparticles have a spherical-like morphology. The optical study shows notable alterations in the absorption spectra with Mn doping. The correlation potential was calculated using the band structure and density of states (DOS) by employing the density functional theory (DFT) method using the BURAI GUI of Quantum ESPRESSO. Remarkably, a significant enhancement in the optical properties was observed with the Mn doping, indicating the successful tuning of the bandgap and the potential for creating nanoscale optoelectronics materials. Such insights are valuable in understanding the underlying physics in order to guide the functional nanomaterials' design for various next-generation technological applications.

INTRODUCTION

Nanotechnology has emerged as a revolutionary field with profound implications across various scientific disciplines and industrial sectors. For numerous semiconducting applications, including gas sensors, biosensors, photodetectors, light emitters, non-volatile storage devices, and magnetic storage devices [1-7], nanoparticles, especially those based on copper oxide, are desirable. Due to its responsiveness to a relatively small magnetic field, CuO has found widespread use in supercapacitors [8]. Copper oxide (CuO) is a *p*-type semiconductor with a narrow bandgap of 1.2-1.9 eV having antiferromagnetic properties [9]. Recent studies have shown that the CuO photonic characteristics make it a promising candidate for a room-temperature ferromagnetic material [10,11]. Doping CuO with transition metal elements has garnered significant attention due to its exceptional properties, which can be precisely tailored for diverse applications. Transition metal-doped wide bandgap semiconductors exhibit ferromagnetism at room temperature, as discovered by Z. Yu et al. [12]. It is a prime contender for low-cost photovoltaic applications due to its narrow bandgap energy, low price, non-toxicity, and high optical absorption coefficient [13]. Despite contentious methods being proposed to explain the magnetisation of nanoscale CuO, little is known about it. For example, CuO nanoparticles with an unpaired electron spin on their surface exhibit ferromagnetism at room temperature, as reported by Elsharawy et al. [14]. According to studies by Gao et al. [15] and K. Tamizh et al. [16], oxygen vacancies (*Vo*) at the interface or shell may be responsible for the magnetic characteristics of CuO nanoparticles.

Furthermore, numerous studies of transition metals doped with CuO have shown that their chemical and physical properties are affected. Nickel [17], iron [18], magnesium [19], zinc [20], cobalt, manganese [21], and other dopants have been found to influence the efficiency of copper oxide nanostructures. Manganese is thought to improve the nanostructures' visible light absorption by establishing an additional energy state within the bandgap [22]. This is a transitional state for charged particles travelling between bands. Even though many studies on Mn-doped CuO nanostructures have already been conducted, using DFT studies to combine the theoretical and experimental efforts aimed at providing a better understanding of the role of Mn-doping, particularly of its band structure and density of the state properties, more details still need to be investigated. This study explores the multifaceted nature of Mn-doped CuO nanoparticles by examining their structural and

optical properties. By comprehensively understanding the interplay between these properties, we can advance the design and development of advanced nanomaterials with tailored functionalities. Such advancements hold immense promise in addressing the current technological challenges while providing innovative solutions for the future. In this context, we present a detailed analysis of the synthesis process, characterisation techniques, and experimental results obtained for Mn-doped CuO nanoparticles. The findings of this investigation can contribute significantly to the growing body of knowledge in nanoscience and nanotechnology, ultimately driving the realisation of cutting-edge applications that harness the full potential of Mn-doped CuO nanoparticles.

EXPERIMENTAL METHODS

Pure CuO nanoparticles (NPs) were produced using a sol-gel method. In 20 mL of methanol, 5 g of Cu $(NO_3)_{2.3}H_2O$ was dissolved. To aid in the gel formation, the solution was mixed and appropriately dissolved for 1 hour before being stored for 2 days and then dried in an oven at 200 °C for two hours. After that, the dried powders were calcined at 500 °C for 10 min using a microwave sintering system with a heating and cooling rate of 50 degrees per minute. Then the same procedure was used for CuO: Mn, except 0.2 wt. % of $Mn(NO_3)_{24}H_2O$ was added as a dopant. To examine the differences between the pure and Mn-doped CuO NPs, a powder XRD (X-ray diffractometer) was used. A selective area electron diffraction (SAED) analysis and high-resolution transmission electron microscopy (TEM, JEM-2100F) were used to determine the *d*-spacing of the Mn-doped CuO nanoparticles. Field Emission Scanning Electron Microscopy (FE-SEM) (JSM7600F) validated the structure and composition of both the pure and Mn-doped CuO NP. BURAI software was employed to design the band structure and density of state for the Mn-doped CuO sample.

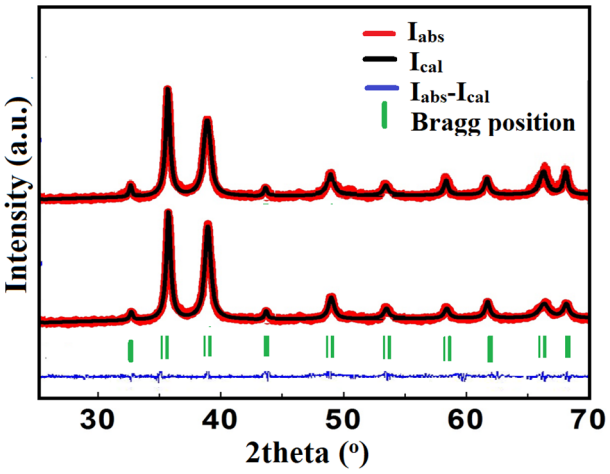

Figure 1. Rietveld refinement profile of the XRD data of the fabricated nanoparticles.

RESULTS AND DISCUSSION

The structure and crystallite size of the pure and doped CuO samples were examined using XRD measurements. The pure and Mn-doped CuO powder diffractograms are shown in Figure 1 over the 20° to 70° range. Nine diffraction peaks were found for the pure and Mn-doped CuO samples matching with the standard JCPDS No.048-1548 of the CuO crystal well [23]. The recorded diffractogram demonstrates that the monoclinic phase with a space group of C2/c was effectively created in the investigated samples. The lack of additional peaks and the observation of the usual peaks of monoclinic CuO indicate that the synthesised material developed in a single phase. Interestingly, the diffraction peaks of the Mn^{2+} doped CuO samples and pure CuO samples seemed to be identical, suggesting that the Mn^{2+} dopant ions, which have a comparable ionic radius (0.074 nm) to the host ion Cu^{2+} (0.073 nm), did not influence the phase and texture of the parent material [24]. Unlike interstitial sites, dopant ions occupy a lattice site, eliminating the possibility of second-phase growth in the material. Furthermore, the diffraction peaks of the Mn-doped CuO are stronger and narrower than those of the pure CuO, showing that Mn-doping increases the crystallinity while decreasing the crystallite size [25]. When the tiny host ion Cu^{2+} is replaced with the significant dopant Mn^{2+} ion, the d-spacing changes, resulting in substantial peaks shifting in the doped CuO, both samples had extremely crisp diffraction peaks, indicating that the materials were created with high crystallinity. By evaluating the diffraction peaks of both prepared materials, the grain size (G), dislocation density (and % crystallinity) could be calculated using the relationships mentioned in Equations 1, 2, and 3, respectively [26-28], and the obtained parameters are reported in Table 1.

Table 1. Crystallographic properties of the pure and Mn-doped CuO samples measured at room temperature and estimated from the XRD data analysis.

Sample	2theta (°)	FWHM (°)	d_{hkl} (nm)	*Dp* (nm)	Crystallinity (%)	Dislocation density
CuO	36.545	0.211637	2.456742	41.31	73.17	0.0028
CuO : Mn	36.347	0.250641	2.512601	34.86	74.58	0.0033

$$Dp = \frac{K\lambda}{\beta \cos\theta} \quad (1)$$

$$\delta = \frac{1}{(G\,S)^2} \quad (2)$$

$$\text{Crystallinity (\%)} = \frac{\text{Area under the crystlline peaks}}{\text{Area of all peaks}} \times 100 \quad (3)$$

As revealed by the structural refinement, the pure and Mn-doped CuO samples crystallise in the monoclinic C2/c space group, as shown in Figure 2a. Cu^{2+} is linked to four equivalent O^{2-} atoms in a square co-planar shape. Two shorter (1.95746 Å) and two longer (1.95478 Å) Cu–O bond lengths exist. O^{2-} is bound to four comparable Cu^{2+} atoms to form an OCu_4 tetrahedra mixture with shared edges and corners. One of the most important results of the X-ray crystallography is a three-dimensional Fourier map, which is made by analysing the X-ray diffraction data. This Fourier map shows how the electrons are spread out in the CuO crystal. It is a very important part of figuring out the atomic structure of the material being studied. If we know the electron density map, we can figure out how the atoms are arranged in the crystal structure in three dimensions. This process is necessary to understand the crystal structure and learn about the features and behaviour of the material. Figure 2a shows how the data from the structure refinement can be used with the G Fourier software to make a 3D Fourier map for the electron density. An electron density

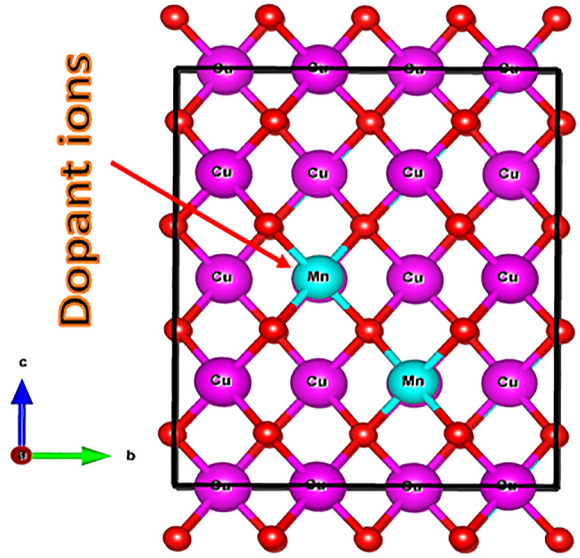

a)

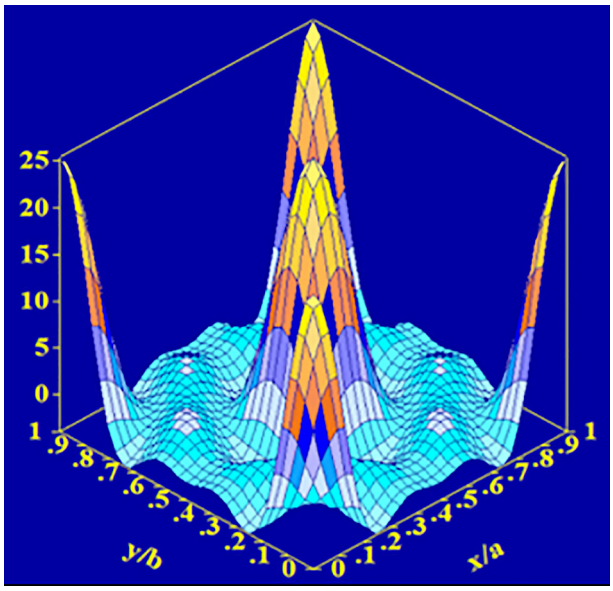

b)

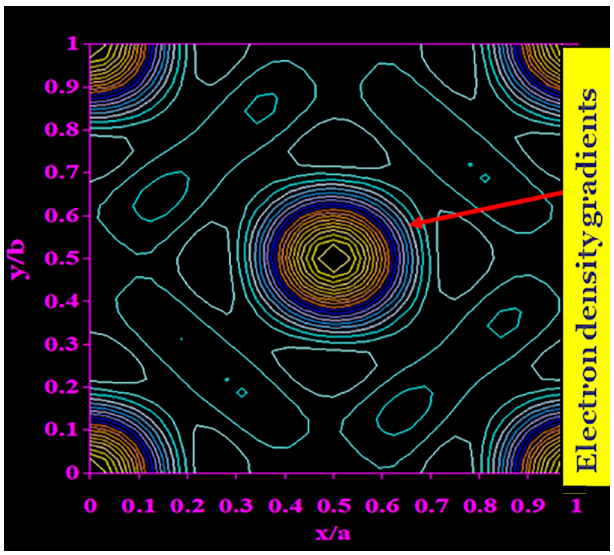

c)

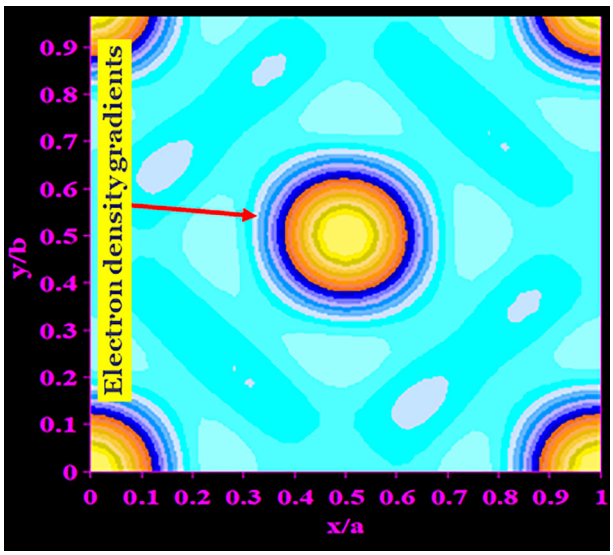

d)

Figure 2. Crystal structures of the Mn-doped CuO crystal (a), 3D Fourier map for the electron density (b), and their 2D contour maps in the Mn-doped CuO crystal (c, d).

diagram, also called an electron density map or plot, is a picture of how the electrons in a crystal lattice are spread out. It is often used in crystallography to see how electrons are packed together and to study how they are arranged around the atomic nuclei. In X-ray diffraction, for example, the electron density map of CuO (Figure 2b) is an essential tool for figuring out how the crystal is built in three dimensions. It is made by looking at the diffraction pattern from X-ray crystallography studies and figuring out what it means. Figures 2b and 2c show the number of electrons by different colours or outline lines. It is a valuable tool for figuring out how other materials are put together and what their qualities are at the atomic level.

For the diffraction pattern, the atomic structure factor (F_{hkl}) is shown as [29-30]:

$$F_{hkl} = \int_0^a \int_0^a \int_0^a \rho_0 (x, y, z) \exp\{2\pi i (hx + ky + lz)\} dx\, dy\, dz \quad (4)$$

The electron density is obtained using an inverse Fourier transform based on the equation mentioned above:

$$\rho (x, y, z) = \frac{1}{V} \sum F_{hkl} \exp\{-2\pi i (hx + ky + lz)\} \quad (5)$$

Usually, areas with more electrons are shown in yellow or thick contour lines, while areas with fewer electrons are shown in lighter colours or with thinner contour lines. This image shows how the atoms are arranged and connected and if there are lone pairs or areas with high electron concentrations in the crystal. It can also show if a crystal structure has disorganised areas around the molecule in the middle. We can note that the electron density map shows how the electrons are spread out on average in the crystal or molecule. It does not show how the electrons are moving or where they are going though.

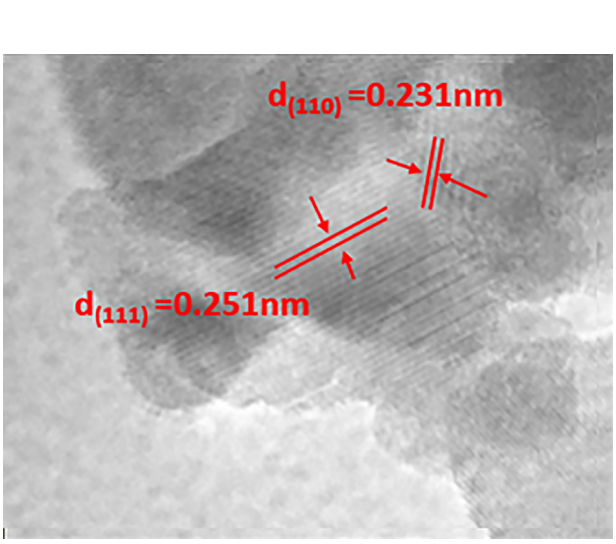

a)

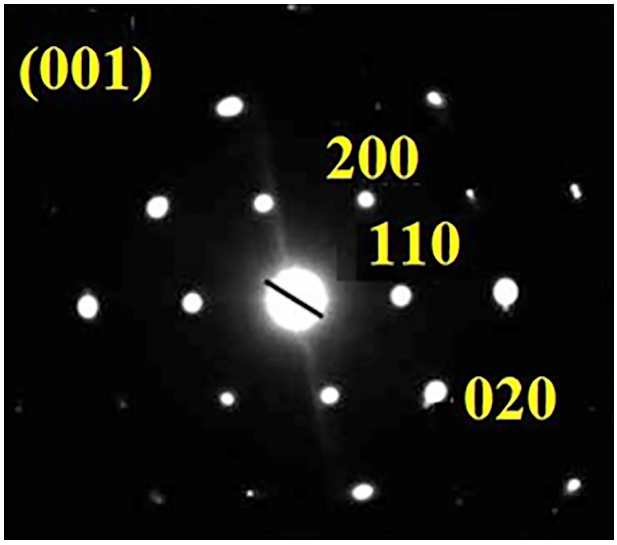

b)

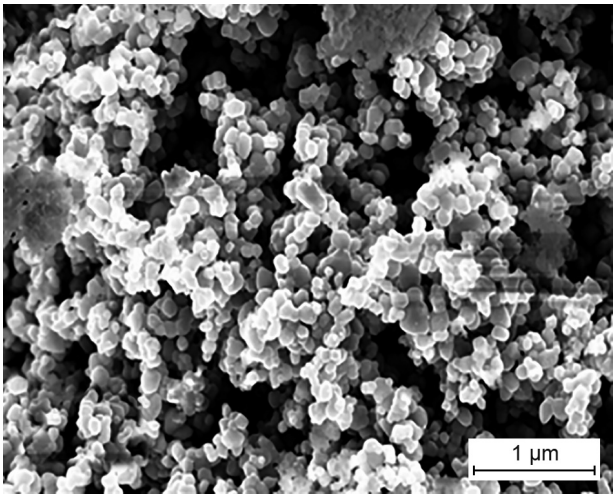

c)

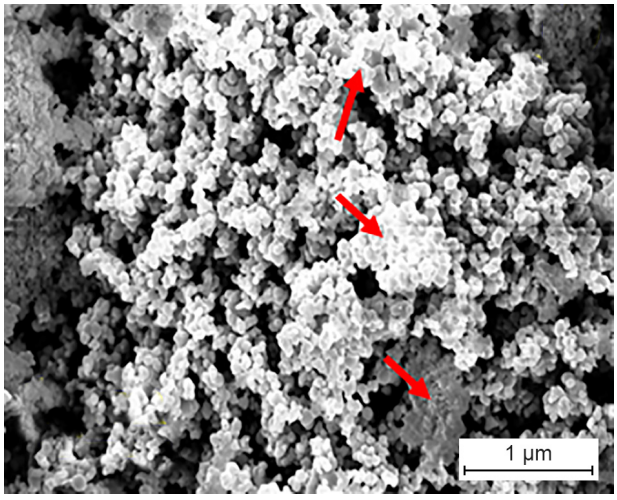

d)

Figure 3. HRTEM images of the Mn-doped CuO sample (a), heir SAED patterns (b), SEM images of the pure and Mn-doped CuO nanoparticles (c, d).

Figure 3a shows an image of the Mn-doped CuO taken using a high-resolution transmission electron microscope (HRTEM). This image reveals two different interplanar distances related to the planes (101) and (111). Figure 3b shows that CuO nanoparticles are polycrystalline based on their SAED patterns. In this way, lattice fringes typical for CuO nanoparticles are demonstrated. The surface morphology is examined by the FE-SEM characterisation method. The surface morphology dynamically tunes the physical characteristics of the produced materials. Figure 3c-d shows the FE-SEM images of the pure and Mn-doped CuO nanoparticles at the same magnification. They are perfectly controlled in size, form, and internal structure. The Image j software was used to calculate the average grain size of the pure and Mn-doped CuO host lattice samples. After doping, the average grain size decreased from roughly 46.24 to 40.76 nm. Furthermore, the FE-SEM images show that the CuO nanoparticles with well-defined shapes have some nanoparticle aggregation, which increases in the doped samples compared to the pure ones. The aggregation increases demonstrating that the Mn doping significantly influences the morphological features.

The energy-dispersive X-ray (EDX) spectra and elemental analysis of the pure and Mn-doped CuO nanoparticles were determined using the X-ray energy-dispersive spectroscopy (EDS) connected to the field emission scanning electron microscope. Only the existence of the elements copper and oxygen was verified. The quality of the produced samples and the presence of all the components are confirmed by the EDX profiles in Figure 4a, b.

The UV/visible absorption spectra of the pure and Mn-doped CuO lattice were measured in the 200-1100 nm wavelength range, as displayed in Figure 5a. CuO materials with Mn doping and pure CuO materials exhibit high absorbance, but the Mn-doped CuO material also exhibits a redshift in the absorption edge. This redshift indicates that the Mn-dopant is responsible for reducing the bandgap by developing a sub-energy level in the bandgap of the CuO host. The decrease in the bandgap permits the Mn-doped sample to absorb to a higher degree in the UV/visible spectrum. The absorbance spectra enable us to estimate the optical gap energy values using the Tauc formula [31,32].

$$(\alpha h \upsilon)^n = A\,(h\nu - E_g) \tag{6}$$

where A is the absorbance, $h\nu$ is the photon energy, n is a number that relies on the electronic transition nature (n = 1/2 in our sample), and E_g is the optical bandgap energy. The Tauc plots for the pure and Mn-doped CuO materials are displayed in Figure 5b.

One might estimate the optical band gap value for a particular sample by extending the linear section of the sample's Tauc plot to the x-axis. According to the calculations, the computed bandgap energies for the pure and Mn-doped CuO material are 2.11 eV and 1,80 eV, respectively. Our Mn-doped CuO material is expected to absorb the maximum light quantity and generate reduced bandgap energy. When the Mn-doped the CuO, the Mn introduces additional energy levels within the band structure. The specific effect on the bandgap energy depends on the concentration of the Mn atoms and their arrangement in the lattice. There are several possible reasons behind the tuning in the bandgap energy of CuO after Mn doping; the Mn atoms can introduce impurity states in the band structure, which create new energy levels within the bandgap. These impurity states can act as intermediate energy levels for electrons, allowing them to transition between the valence and conduction bands with lower energy. This effectively reduces the bandgap energy, as shown in Figure 5b, consistent with literature reports [33-35].

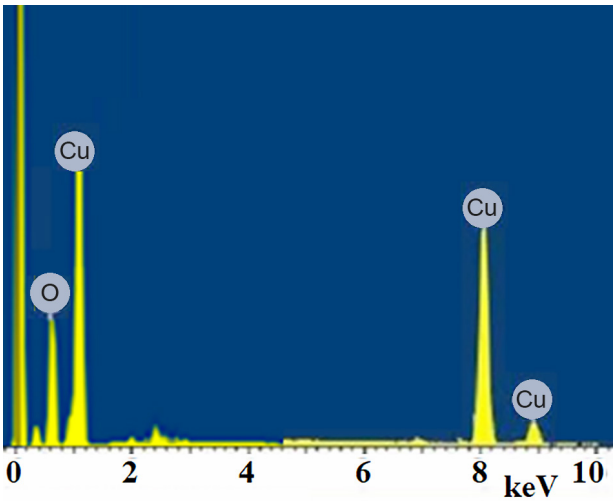

b)

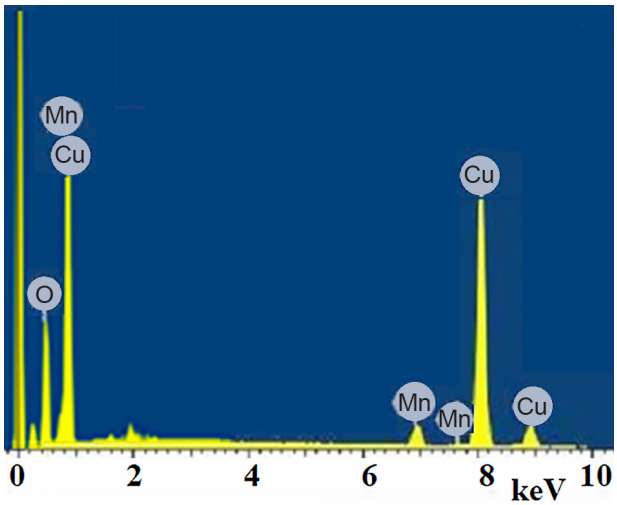

c)

Figure 4. EDX spectra of: a) the pure, b) Mn-doped CuO nanoparticles.

It is important to mention that the DFT calculations are widely used to understand the electronic and structural properties of materials at the quantum level. This analysis may provide valuable insights into the mechanisms responsible for the changes in the electronic structure upon the Mn doping in CuO, which can be crucial for understanding the material's behaviour and potential applications. However, it is essential to corroborate these theoretical findings with experimental data to validate the accuracy and reliability of the DFT-based predictions. Comparing the theoretical results with the experimental measurements will provide a comprehensive understanding of the material's properties and pave the way for further investigations and applications in the future. We have provided a detailed analysis of the theoretical results obtained from the DFT calculations and structural refinement for the Mn-doped CuO. Based on the information we mentioned in the structural analysis, it is evident that the Mn 3d states play a significant role in influencing the electronic structure and bandgap of the material. Let's summarise the key points from analysis: Mn 3d State Contributions: (i) The presence of Mn 3d states in the electronic structure of Mn-doped CuO substantially impacts the valence band region. This contribution is likely responsible for altering the material's electronic properties. (ii) Active Transitions: The transitions involving the Mn 3d states in the Mn^{2+} ions are likely to be actively participating in the electronic processes within the material. These transitions can lead to changes in the band structure and bandgap. (iii) sp-d Exchange Interactions: The strong exchange interactions between the band electrons and the localised 'd' electrons of the Mn^{2+} dopant play a crucial role in modifying the electronic properties. These interactions can influence the band structure and bandgap. (iv) Hybridization with O 2p States: The position of the Mn 3d states above the valence band maxima (VBM) causes them to hybridise with the O 2p states. This hybridisation effect results in the pulling up of the VBM, which decreases the bandgap after the Mn doping. The combined effect of the factors mentioned above results in the observed decrease in the bandgap of the Mn-doped CuO compared to the pure case.

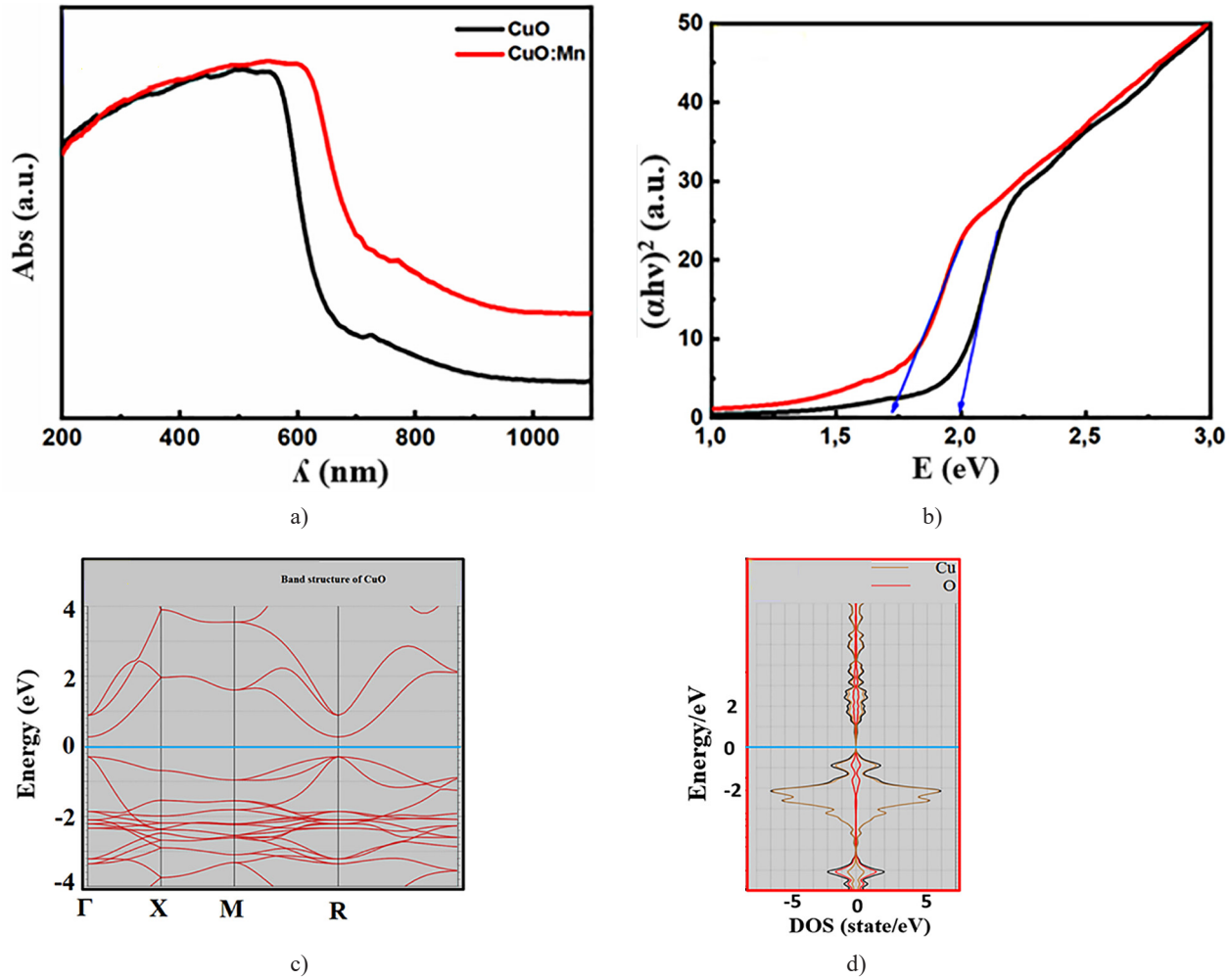

Figure 5. UV-spectra (a) and Tauc plot (b) of the pure and Mn-doped CuO lattice and the band structure and density of the state diagrams for the Mn-doped CuO crystal (c, d).

CONCLUSION

In conclusion, this study investigated Mn-doped CuO nanoparticles' structural and optical properties. The results showed that the Mn-doped CuO nanoparticles had a well-monoclinic structure without a second phase, indicating successful doping without any significant changes in the CuO crystal lattice. The optical study revealed notable alterations in the absorption spectra with the Mn doping. The density functional theory (DFT) method was employed to calculate the correlation potential using the band structure and density of states (DOS). Remarkably, a significant enhancement in the optical absorption in the visible region was observed with the Mn doping, indicating the successful introduction of transition metal dopants and the potential for creating nanoscale optoelectronic materials. These findings demonstrate the potential for tuning the physical and chemical properties of CuO nanoparticles through transition metal doping, which could have important implications for various technological applications, including data storage, catalysis, and photovoltaics devices. Further research is needed to fully understand the underlying physics and guide the design of functional nanomaterials for these applications.

Acknowledgment

The author expresses gratitude to the Researchers Supporting Project (RSPD2023R759), King Saud University, Riyadh, Saudi Arabia, for providing financial support.

REFERENCES

1. Geng W., Ma Z., Zhao Y., Yang J., He X., Duan L., et al. (2020): Morphology-dependent gas sensing properties of CuO microstructures self-assembled from nanorods. *Sensors and Actuators B: Chemical,* 325, 128775. Doi: 10.1016/j.snb.2020.128775
2. Lillo-Ramiro J., Guerrero-Villalba J. M., Mota-González M. D. L., Aguirre-Tostado F. S., Gutiérrez-Heredia G., Mejía-Silva I., Carrillo-Castillo A. (2021): Optical and microstructural characteristics of CuO thin films by sol-gel process and introduction in non-enzymatic glucose biosensor applications. *Optik*, 229, 166238. Doi: 10.1016/j.ijleo.2020.166238
3. Ji Y., Jung U., Xian Z., Kim D., Yu J., Park J. (2020): Ultraviolet photodetectors using hollow *p*-CuO nanospheres/n-ZnO nanorods with a pn junction structure. *Sensors and Actuators A: Physical,* 304, 111876. Doi: 10.1016/j.sna. 2020.111876
4. Salih E. Y., Bashir M. B. A., Rajpar A. H., Badruddin I. A. (2022): Fabrication and characterization of porous Si/CuO film for visible light MSM photodetector: The effect of post-processing temperature. *Ceramics International*, *48*(7), 9965-9972. Doi: 10.1016/j.ceramint.2021.12.203
5. Zhou Y., Li J., Peng W., Liu Y., Zhang J., Xiang G., et al. (2021): Near-white light-emitting diode from p-CuO/n-GaN heterojunction with an i-CuO electron blocking layer. *Journal of Alloys and Compounds*, *867*, 159145. Doi: 10.1016/j.jallcom.2021.159145
6. Hussain I., Iqbal S., Hussain T., Cheung W. L., Khan S. A., Zhou J., et al. (2022): Zn–Co-MOF on solution-free CuO nanowires for flexible hybrid energy storage devices. *Materials Today Physics*, *23*, 100655. Doi: 10.1016/j.mtphys.2022.100655
7. Ganesan K. P., Amaliroselin, A., Joseph Panneer Doss, I., Anandhan, N., Ramesh, R., Prabhu, S., et al. (2021): High-performance energy storage of highly saturated ferromagnetic cobalt-doped cuprous oxide thin films. *Journal of Materials Science: Materials in Electronics*, *32*, 7509-7527. Doi: 10.1007/s10854-021-05463-y
8. Hussain I., Sahoo S., Hussain T., Ahmad M., Javed M. S., Lamiel C., et al. (2023): Theoretical and Experimental Investigation of In Situ Grown MOF-Derived Oriented Zr-Mn-oxide and Solution-Free CuO as Hybrid Electrode for Supercapacitors. *Advanced Functional Materials*, *33*(7), 2210002. Doi: 10.1002/adfm.202210002
9. Mote V. D., Lokhande S. D., Kathwate L. H., Awale M. B., Sudake Y. (2023): Structural, optical and magnetic properties of Mn-doped CuO nanoparticles by coprecipitation method. *Materials Science and Engineering: B*, *289*, 116254. Doi: 10.1016/j.mseb.2022.116254
10. Singh S., Kumar V., Tyagi S., Saxena N., Khan Z. H., Kumar P. (2023): Room temperature ferromagnetism in metal oxides for spintronics: A comprehensive review. *Optical and Quantum Electronics*, *55*(2), 123. Doi: 10.1007/s11082-022-04325-z
11. Jamal M., Billah M. M., Ayon S. A. (2023): Opto-structural and magnetic properties of fluorine-doped CuO nanoparticles: An experimental study. *Ceramics International*, *49*(6), 10107-10118. Doi: 10.1016/j.ceramint.2022.11.194
12. Yu Z., Deng C., Kong S., Hui H., Guo J., Zhao Q., et al. (2022): Transition metal-doped chalcogenide perovskite magnetic semiconductor $BaZrS_3$. *Journal of Magnetism and Magnetic Materials*, *563*, 169886. Doi: 10.1016/j.jmmm.2022.169886
13. Singh B. P., Chaudhary M., Kumar A., Singh A. K., Gautam Y. K., Rani S., Walia R. (2020): Effect of Co and Mn doping on the morphological, optical and magnetic properties of CuO nanostructures. *Solid State Sciences*, *106*, 106296. Doi: 10.1016/j.solidstatesciences.2020.106296
14. Elsharawy A. I., Yakout S. M., Wahba M. A., Abdel-Shafi A. A., Khalil M. S. (2023): Transition-metal blends incorporated into CuO nanostructures: Tuning of room temperature spin-ferromagnetic order. *Solid State Sciences*, *139*, 107166. Doi: 10.1016/j.solidstatesciences.2023.107166
15. Gao D., Zhang J., Zhu J., Qi J., Zhang Z., Sui W., et al. (2010): Vacancy-mediated magnetism in pure copper oxide nanoparticles. *Nanoscale Research Letters*, *5*, 769-772. Doi: 10.1007/s11671-010-9555-8
16. Selvi K. T., Mangai K. A., Priya M., Sagadevan S. (2021): Enhanced electrical and magnetic properties of CuO/MgO nanocomposites. *Chemical Physics Letters*, *765*, 138320. Doi: 10.1016/j.cplett.2021.138320
17. Chandrasekar M., Subash M., Logambal S., Udhayakumar G., Uthrakumar R., Inmozhi C., et al. (2022): Synthesis and characterization studies of pure and Ni doped CuO nano-

particles by hydrothermal method. *Journal of King Saud University-Science*, *34*(3), 101831. Doi: 10.1016/j.jksus.2022.101831

18. Yildirimcan S. (2023): Effect of ageing on electrical properties of Fe-doped CuO thin films deposited by spin coating technique. *Indian Journal of Physics*, *97*(6), 1707-1716. Doi: 10.1007/s12648-022-02511-z
19. Azharudeen A. M., Badhusha A., Khan M. S., Prabhu S. A., Kumar P. V., Karthiga R., et al. (2022): Solar power light-driven improved photocatalytic action of Mg-doped CuO nanomaterial modified with polyvinylalcohol. *Journal of Nanomaterials*, *2022*. Doi: 10.1155/2022/2430840
20. Kumar P., Mathpal M. C., Prakash J., Viljoen B. C., Roos W. D., Swart H. C. (2020): Band gap tailoring of cauliflower-shaped CuO nanostructures by Zn doping for antibacterial applications. *Journal of Alloys and Compounds*, *832*, 154968. Doi: 10.1016/j.jallcom.2020.154968
21. Yakout S. M. (2021): Tri-dopants (Mn, Fe, Co): superior room temperature ferromagnetic properties of p-type CuO. *Materials Chemistry and Physics*, *273*, 125110. Doi: 10.1016/j.matchemphys.2021.125110
22. Iqbal M., Thebo A. A., Shah A. H., Iqbal A., Thebo K. H., Phulpoto S., Mohsin M. A. (2017): Influence of Mn-doping on the photocatalytic and solar cell efficiency of CuO nanowires. *Inorganic Chemistry Communications*, *76*, 71-76. Doi: 10.1016/j.inoche.2016.11.023
23. Wang Y. T., Zhang X. T., Xu J. B., Shen Y., Wang C. A., Li, F. W., et al. (2021): Fabrication and characterization of Al–CuO nanocomposites prepared by sol-gel method. *Defence Technology*, *17*(4), 1307-1312. Doi: 10.1016/j.dt.2020.06.029
24. Jayaprakash J., Srinivasan N., Chandrasekaran P., Girija E. K. (2015): Synthesis and characterization of cluster of grapes like pure and Zinc-doped CuO nanoparticles by sol-gel method. *Spectrochimica Acta Part A: Molecular and Biomolecular Spectroscopy*, *136*, 1803-1806. Doi: 10.1016/j.saa.2014.10.087
25. Pramothkumar A., Senthilkumar N., Mercy Gnana Malar K. C., Meena M., Vetha Potheher I. (2019): A comparative analysis on the dye degradation efficiency of pure, Co, Ni and Mn-doped CuO nanoparticles. *Journal of Materials Science: Materials in Electronics*, *30*, 19043-19059. Doi: 10.1007/s10854-019-02262-4
26. Yousaf S., Zulfiqar S., Din M. I., Agboola P. O., Aboud M. F. A., Warsi M. F., Shakir I. (2021): Solar light irradiated photocatalytic activity of ZnO–NiO/rGO nanocatalyst. *Journal of Materials Research and Technology*, *12*, 999-1009. Doi: 10.1016/j.jmrt.2021.03.012
27. Ashraf N., Aadil M., Zulfiqar S., Sabeeh H., Khan M. A., Shakir I., et al. (2020): Wafer-like CoS architectures and their nanocomposites with polypyrrole for electrochemical energy storage applications. *ChemistrySelect*, *5*(27), 8129-8136. Doi: 10.1002/slct.202001305
28. Tamam N., Aadil M., Hassan W., Ejaz S. R., Najm Z. M., Alsafari I. A., et al. (2022): Surfactant assisted synthesis of nanostructured Mn-doped CuO: An efficient photocatalyst for environmental remediation. *Ceramics International*, *48*(20), 29589-29600. Doi: 10.1016/j.ceramint.2022.06.213
29. Alkathy M. S., Zabotto F. L., Milton F. P., Botero E. R., Gatasheh M. K., Goud J. P., Eiras J. A. (2023): Effect of sintering temperature on structural, electrical, and ferroelectric properties of neodymium and sodium co-doped barium titanate ceramics. *Journal of Materials Science: Materials in Electronics*, *34*(14), 1144. Doi: 10.1007/s10854-023-10576-7
30. Hooda N., Sharma R., Hooda A., Khasa S. (2022): Investigations on structure, dielectric and multiferroic behavior of (1− x) BaFe12O19–(x) BaTiO3 composites. *Journal of Materials Science: Materials in Electronics*, *33*(20), 16441-16465. Doi: 10.1007/s10854-022-08537-7
31. Rahman A., Zulfiqar S., Haq A. U., Alsafari I. A., Qazi U. Y., Warsi M. F., Shahid M. (2021): Cd-Gd-doped nickel spinel ferrite nanoparticles and their nanocomposites with reduced graphene oxide for catalysis and antibacterial activity studies. *Ceramics International*, *47*(7), 9513-9521. Doi: 10.1016/j.ceramint.2020.12.085
32. Aadil M., Zulfiqar S., Shahid M., Haider S., Shakir I., Warsi M. F. (2020): Binder free mesoporous Ag-doped Co_3O_4 nanosheets with outstanding cyclic stability and rate capability for advanced supercapacitor applications. *Journal of Alloys and Compounds*, *844*, 156062. Doi: 10.1016/j.jallcom.2020.156062
33. Jiang T., Kong J., Wang Y., Meng D., Wang D., Yu M. (2016): Optical and Photocatalytic properties of Mn-doped CuO nanosheets prepared by hydrothermal method. *Crystal Research and Technology*, *51*(1), 58-64. Doi: 10.1002/crat.201500152
34. Tamam N., Aadil M., Hassan W., Ejaz S. R., Najm Z. M., Alsafari I. A., et al. (2022): Surfactant assisted synthesis of nanostructured Mn-doped CuO: An efficient photocatalyst for environmental remediation. *Ceramics International*, *48*(20), 29589-29600. Doi: 10.1016/j.ceramint.2022.06.213
35. Rahaman R., Sharmin M., Podder J. (2022): Band gap tuning and p to n-type transition in Mn-doped CuO nanostructured thin films. *Journal of Semiconductors*, *43*(1), 012801. Doi: 10.1088/1674-4926/43/1/012801